

The X-ray Spectrum of the Rapid Burster using the *Chandra* HETGS

H.L. Marshall¹, R. Rutledge², D.W. Fox¹, J.M. Miller¹, R. Guerriero³, E. Morgan¹, M. van der Klis⁴,
L. Bildsten⁵, T. Dotani⁶, W.H.G. Lewin¹

hermanm@space.mit.edu

ABSTRACT

We present observations of the Rapid Burster (RB, also known as MXB 1730–335) using the *Chandra* High Energy Transmission Grating Spectrometer. The average interval between type II (accretion) bursts was about 40 s. There was one type I (thermonuclear flash) burst and about 20 “mini-bursts” which are probably type II bursts whose peak flux is 10-40% of the average peak flux of the other type II bursts. The time averaged spectra of the type II bursts are well fit by a blackbody with a temperature of $kT = 1.6$ keV, a radius of 8.9 km for a distance of 8.6 kpc, and an interstellar column density of 1.7×10^{22} cm⁻². No narrow emission or absorption lines were clearly detected. The 3σ upper limits to the equivalent widths of any features are < 10 eV in the 1.1-7.0 keV band and as small as 1.5 eV near 1.7 keV. We suggest that Comptonization destroys absorption features such as the resonance line of Fe XXVI.

Subject headings: X-ray sources, individual:MXB 1730–335

1. Introduction

The Rapid Burster (RB) is a recurrent transient low-mass X-ray binary with an X-ray burst phenomenology that makes it unique in the Galaxy. The many idiosyncrasies of the RB are overwhelming, and it is fair to say that we do not understand why the RB, and only the RB, behaves so differently from all other low mass X-ray binaries (LMXBs). For a detailed review see Lewin, Van Paradijs & Taam (1993), hereafter LVT. The RB (MXB 1730–335) is the only low-mass X-ray binary (LMXB) known to produce

¹Center for Space Research, Massachusetts Institute of Technology, Cambridge, MA 02139

²Space Radiation Laboratory, Caltech, MS 220-47, Pasadena, CA 91125

³Department of Physics, United States Military Academy, West Point, NY 10996

⁴Faculty of Mathematics, Computer Science, Physics & Astronomy, University of Amsterdam, the Netherlands

⁵Harvard University, Cambridge, MA 02138

⁶Institute of Space and Astronautical Science, Sagamihara, Kanagawa, 229-8510 Japan

two types of X-ray bursts (Hoffman, Marshall, & Lewin 1978). Type I bursts, which are observed from ~ 40 LMXBs, are due to thermonuclear flashes on the surface of an accreting neutron star. They typically recur on time scales of hours to tens of hours (LVT). Type II bursts are due to accretion instabilities (gravitational potential energy). In the RB, their durations range from ~ 2 to ~ 680 sec, and thousands of short bursts can occur in a single day. The behavior of the type II bursts from the RB is like that of a relaxation oscillator: the type II burst fluence E is roughly proportional to the time interval, Δt , to the following burst (the “ E - Δt ” relation). The time averaged luminosity of the RB is $\sim 10^{37}$ erg s^{-1} during its active periods which typically last for several weeks. The type II burst luminosities at burst maximum range from $\sim 5 \times 10^{37}$ to $\sim 4 \times 10^{38}$ erg s^{-1} (LVT). Henceforward, whenever we use the word “burst(s)”, we mean type II burst(s) unless we specify otherwise.

Among the LMXBs, the RB stands alone in its complex QPO behavior, none of which is understood (LVT). With the *Rossi X-ray Timing Explorer (RXTE)* we may have detected ($> 98\%$ significance) the signature of near coherent 306.5 Hz pulsations in the average power-density spectrum of the first second of 31 Type I bursts (Fox, et al. 2001).

Though we are largely at a loss in our understanding of this system, it is important to remember that there have been occasions that, when the RB became active, it behaved like an ordinary LMXB and then transitioned to rapid bursting. Starting August 5, 1983, no type II bursts were detected but instead a strong persistent X-ray flux and type I bursts were observed for several days Kunieda, et al. (1984); Barr, et al. (1987). In the period November 6–17, 1996, and July 7–10, 1997 (during a total of 18 ksec of *RXTE* observations) the RB again produced only persistent emission and type I bursts at the beginning of its activity cycle.

We are reporting results from the first high resolution X-ray spectral observation of the RB, using the *Chandra* High Energy Transmission Grating Spectrometer (HETGS). A description of the HETGS and its performance are given by Canizares et al. (in preparation). Our objective was to search for spectral emission and absorption features that might distinguish the bursts from the persistent emission. The type II bursts, due to their E - Δt character, are believed to be emission from the surface of the NS. Discovery of any emission or absorption features might then provide a measure of the gravitational redshift at the NS photosphere.

2. Observations and Data Reduction

The RB was observed with the *Chandra* HETGS on 24-25 October 1999 (MJD = JD - 2400000.5 = 51476.2-6.6). The Advanced CCD Imaging Spectrometer (ACIS-S) detector was used for readout and was operated in the so-called “continuous clocking” (CC) mode. This mode is mentioned in the *Chandra* Proposer’s Observatory Guide (p. 101). In this mode, the charge is shifted row by row to the frame storage buffer at 2.84996 ms intervals so the X-ray events are timed to an accuracy of about 3 ms by locating events within the storage buffer, assuming that the event is associated with the target. The total exposure time was 29562.7 s, during which a total of 702 bursts were detected. A few samples of the light curve from zeroth order are shown in Fig.1, which shows a type I burst about 11580 s into the observation. The type I burst

was fairly typical of those discovered by Hoffman, Marshall, & Lewin (1978), having a similar peak flux to that of the type II bursts but with a longer decay time constant.

The median peak burst count rate was about 45 count s^{-1} but the average burst count rate is about a factor of two smaller due to the nearly triangular shapes of the burst profiles. Average burst spectra were determined by selecting events where the count rate over a 1 s interval exceeded 5 count s^{-1} , eliminating only 10% of the total counts in type II bursts while simultaneously reducing the background (see 2.2) by more than a factor of three. A “peak” burst spectrum was also derived by restricting the selection to intervals where the count rate exceeded 30 count s^{-1} , which gave half as many counts as the average spectrum. After removing 82 s containing the type I burst, the exposure time was 4326 s in the average spectrum and 1349 s in the peak spectrum. The average count rate was $23.4 \text{ count s}^{-1}$ for the average spectrum and $39.7 \text{ count s}^{-1}$ in the peak spectrum. In addition to the type I burst there were 18 “mini-bursts” where the peak flux is 10-40% of the peak flux from the remaining bursts which are mostly included in the average spectrum but entirely excluded from the peak spectrum. The first seven of these mini-bursts are shown in Fig.1.

The CC mode introduces complications into the spectral processing. Imaging information along the readout direction is lost in favor of improved event timing. In the timed exposure (TE) mode, the imaging information is used to select the HEG and MEG data for spectral extraction and for the selection of background. In CC mode, only the ACIS pulse height data are used. The MEG and HEG first orders are well separated in energy when at any specific dispersion distance although there is the ambiguity that an event dispersed into 2nd order by the MEG gratings will have the same energy as an HEG photon and dispersed by the same distance. In practice, however, the efficiency of the MEG in 2nd order is a few percent of the HEG efficiency in the 1-10 keV range, so this ambiguity is not an issue.

Background selection for spectral analysis is not simple, so this instrument mode is best suited for bright targets such as the RB during bursts. We cannot define the background spatially so we instead select regions of pulse height as a function of dispersion distance with the same width, ΔE , as used for selecting the source but displaced in energy (see step 10 of the spectral processing). Due to the difficulty in processing and analyzing the CC mode data, we took great care to check our methods using data from other sources observed with this mode, such as the Crab pulsar (observation ID 170) and Cyg X-1 (observation ID 1511).

2.1. Imaging

As stated, there is limited spatial information; we obtain $\sim 1''$ resolution along one dimension of the detector array. In this dimension, when the spacecraft dither and the thermal drifts are removed, the result is a very narrow image of the HETGS zeroth order. It is well fit with a Gaussian of $0.77''$ FWHM, which is consistent with the superb imaging of the *Chandra* mirror assembly if the image is integrated along one dimension.⁷ In order to properly remove the telescope dither, however, we required advancing the times

⁷Although the one dimensional response function is not well documented, one may examine results posted on the web by Dan Dewey: http://space.mit.edu/HETG/technotes/zo_1d/focus_trends.010227.html.

assigned to the events by about 5 s. Other instruments on *Chandra* do not require this timing offset, so we conclude that the offset is an unaccounted fixed timing offset. It was also found to be required for dither correction in all other CC mode observations, including an observation of the Crab pulsar and the pulsar B0540-69 (Kaaret, et al. 2001).⁸

2.2. Spectra

The spectral data were reduced starting from level 1 data provided by the Chandra X-ray Center (CXC) using IDL custom processing scripts; the method is quite similar to processing data from timed exposure (TE) mode but has two wrinkles that make it more difficult. This procedure was successfully verified using CC mode data from Cyg X-1 and is more thoroughly described by Marshall, et al. (in preparation). Briefly, the procedure was to: 1) restrict the event list to the nominal grade set (0,2,3,4, and 6), 2) remove the event streaks in the S4 chip (which are not related to the readout streak and appear in CC and TE mode data alike), 3) compute a projected dispersion distance (x_p , in mm) by correcting for telescope dither along the dispersion direction after applying the timing offset determined using the dither pattern of the zeroth order events along the readout direction (as described in the last section), 4) determine the location of zeroth order, x_{p0} , by fitting a Gaussian to the one dimensional profile, 5) estimate the event wavelength $m\lambda = P(x_p - x_{p0}) / (R \cos \theta)$ (where P is the grating period, m is the dispersion order, R is the Rowland distance in mm, and θ is the clocking angle of the MEG or HEG), 6) correct event energies for detector node-to-node gain variations, 7) select ± 1 order events in order to minimize background using $|E_{ACIS} * m\lambda / (hc)| - 1 < \Delta$ where E_{ACIS} is the event energy inferred from the ACIS pulse height, and Δ is a function of λ , ranging from 0.025 at 1 Å to 0.15-0.20 for $\lambda > 6$ Å, 8) eliminate events in bad columns where the counts in an histogram deviate by 5σ from a 50 pixel running median,⁹ 10) select background events by applying a E_{ACIS} criterion similar to that applied to select source events but accepting events in the range Δ to 2Δ , 11) bin MEG (HEG) events at 0.01 Å (0.005 Å), 12) eliminate data affected by detector gaps, and 13) generate and apply an instrument effective area based on the pre-flight calibration data and a set of correction polynomials derived from the CC mode observation of Cyg X-1 (Marshall et al., in preparation).

The time averaged spectra of the type II bursts are shown in Figs. 2 and 3. The data have been adaptively rebinned to give a nearly constant signal/noise ratio better than 10 except in the bin at the lowest energy. A blackbody model has been fit to the data and overplotted in the upper panel. A 5% systematic error was added to the uncertainties in quadrature so that the χ^2 came out to 1.00. This model of the uncertainties is not precisely correct because there are correlations between the systematic error in adjacent bins. One

⁸Note that Kaaret, et al. (2001) misstated the sign of the correction. A constant offset of about 5 s must be *subtracted* from the times of events in order to match the time of the aspect system. Of five CC mode observations we have processed, the sign and magnitude of the offset is the same. We estimate that the offset time is accurate to about 0.5s.

⁹There were many bad columns, especially on the S2 and S4 chips. The cause may be a poor on-board bias map calculation (Peter Ford, private communication). These mostly affect the dispersed spectrum below 1 keV so they have a negligible effect on our spectral results.

systematic error is due to the difference between the background spectra derived from events with E_{ACIS} larger than $(hc)/(m\lambda)$ compared to those events where E_{ACIS} is smaller than $(hc)/(m\lambda)$. The background is less than 10% of the signal for $1.5 < E < 8.0$ keV. The systematic errors are small in this energy band so that their true dependence on energy will not have a significant effect on our results.

The burst peak spectra are well fit by a blackbody with $kT = 1.590 \pm 0.016$ keV with a radius of 8.88 ± 0.14 km for a distance of 8.6 kpc, and the interstellar column density, N_H , was measured to be $1.81 \pm 0.03 \times 10^{22}$ cm⁻². The fit to the burst average spectra gave similar values for the temperature and N_H , 1.577 ± 0.012 keV and $1.74 \pm 0.03 \times 10^{22}$ cm⁻², but the fitted radius was significantly smaller, 6.54 ± 0.08 km. The uncertainties determined in the fit are indicative of the high counting statistics ($> 10^5$ counts) but would increase as one takes systematic errors into account; we estimate that the uncertainties should be regarded as good to a factor of 2. In principle, we would be able to verify the fitted value of N_H by measuring the ionization edges due to Mg and Si at 1.30 and 1.84 keV, respectively. With large N_H and relatively low source flux below the spectral peak of the blackbody emission, the flux is insufficient to measure the optical depths at the edges to better than a factor of 2, so we cannot obtain a useful independent constraint on N_H .

We searched the time-averaged spectra for narrow absorption and emission features and found several candidates. All candidates were found to be spurious, however, by comparing the HEG and MEG spectra and the +1 orders to the -1 orders. The burst peak spectra also showed no features. In Fig. 4, we show estimates of the 3σ limits that can be placed on any emission lines whose widths (FWHMs) are comparable to the instrument resolution. The computation uses the model fitted to the time-averaged HEG and MEG data and the effective areas. We assume that candidate features are only 2 bins wide. The curves are rather smooth, except for locations of chip gaps, so one may derive limits on broader features using these curves until the scale of the feature becomes comparable to that of the instrument calibration uncertainties. Limits on absorption lines are identical when there are a lot of counts but are systematically larger. The 3σ upper limits to the equivalent widths of any features are < 10 eV in the 1.1-7.0 keV band and as small as 1.5 eV near 1.7 keV.

3. Discussion

We find that the color temperature at the peak of the type II bursts is the same as the average color temperature to within the very small statistical uncertainties even though the count rate drops by a factor of two from the average of the burst peaks to the average of all type II bursts. This finding confirms a result that is well established for significantly longer bursts – that the color temperature is not observed to vary significantly during the bursts (Marshall, et al. 1979). Thus, the profile of a type II burst seems to result from variation of the size of the emission region with a maximum of about 9 km. If all emission takes place on the surface of a neutron star, then any smaller apparent radius must result from nonuniformities over the stellar surface; in the simplest geometry, the emission is assumed to emanate from a spot on the surface. During the fainter parts of normal type II bursts and near the peaks of minibursts the observed intensity drops to 10% of the peak so the apparent fraction of the surface, f_a , is about 0.1. Marshall (1982)

computed f_a of an emission region spot covering a true fraction f of the surface for various values of the ratio of the stellar radius to its Schwarzschild radius. For a $1.4 M_\odot$ neutron star with a 7 km radius which is uniformly radiating across its surface, the apparent radius (measured at infinity) is 11 km, so we would infer that the type II emission region covers between 5 and 20% of the surface when faint and an average of 50-85% at burst peak. The endpoints of the allowed range depend on whether the spot is centered on the nearest or farthest points of the surface. Gravitational bending of light trajectories ensures that all bursts can be detected as long as at least 5-10% of the surface radiates, for relatively compact neutron stars.

The main objective of this observation was to determine if there would be emission lines or absorption features that could be used to determine the gravitational redshift of the emission region. At the estimated temperature of the emission region, Fe will be highly ionized, so a significant fraction of the Fe will be He-like Fe XXV, for which the strongest resonance line is at 6.70 keV. If the radiating region is spherically symmetric, then the emission region is a shell at a radius of 7 km and the Fe XXV line will be gravitationally redshifted to about 4.3 keV, where our 3σ upper limit to absorption features is 3 eV. The instrumental resolution is 0.01Å, which is 15 eV at this energy. Pressure broadening of the resonance line due to the Stark effect in a highly ionized, hydrogen-dominated plasma is estimated to be about 4 eV in the rest frame of the gas while fine-structure splitting is of order 21 eV (Paerels, 1997). There is a 30% narrowing to the observed frame due to the gravitational redshift so the line FWHM is expected to be comparable to the instrumental resolution. The thermal line FWHM is smaller, ~ 1 eV. Thus, the upper limit on the column density of Fe XXV is about $8 \times 10^{15} \text{ cm}^{-2}$. For a simple model atmosphere dominated by electron scattering, the column density of Fe to one optical depth is of order $X_{Fe}/\sigma_T = 5 \times 10^{19} \text{ cm}^{-2}$, where X_{Fe} is the abundance of Fe and σ_T is the Thomson cross section. The discrepancy of $\sim 10^4$ leads us to suggest that Compton scattering dominates the spectrum, destroying possible line features.

At the measured color temperature, Comptonization is expected to shift low energy photons to higher energies. The color temperature is systematically larger than the effective temperature of the plasma. The magnitude of this bias is not well determined but can be a factor of 1.5 (cf. LVT). A decrease of the temperature requires a compensating increase of the inferred radius of the emission region, yielding a radius of approximately 20 km. This radius is somewhat larger than observed in other burst sources but still feasible from theoretical standpoint.

This work has been supported in part under NASA grant NAG5-3239, and NASA contracts NAS8-38249, NAS8-39073, and SAO SV1-61010.

REFERENCES

- Barr, P., et al., 1987, A&A176, 69
 Fox, D. et al., 2001, MNRAS, 321, 776
 Hoffman, J.A., Marshall, H.L., and Lewin, W.H.G. 1978, Nature, 271, 630

Kaaret, H., et al., 2001, ApJ, 546, 1159

Kunieda, H., et al., 1984, PASJ 36, 215

Lewin, W.H.G., Van Paradijs, J., and Taam, R. 1993, Space Sci. Rev. 62, 223 (LVT)

Marshall, H.L., Hoffman, J.,A. Doty, J., Lewin, W.H.G., and Ulmer, M.P. 1979, ApJ, 227, 555

Marshall, H.L. 1982, ApJ, 260, 815

Paerels, F. 1997, ApJ, 476, L47

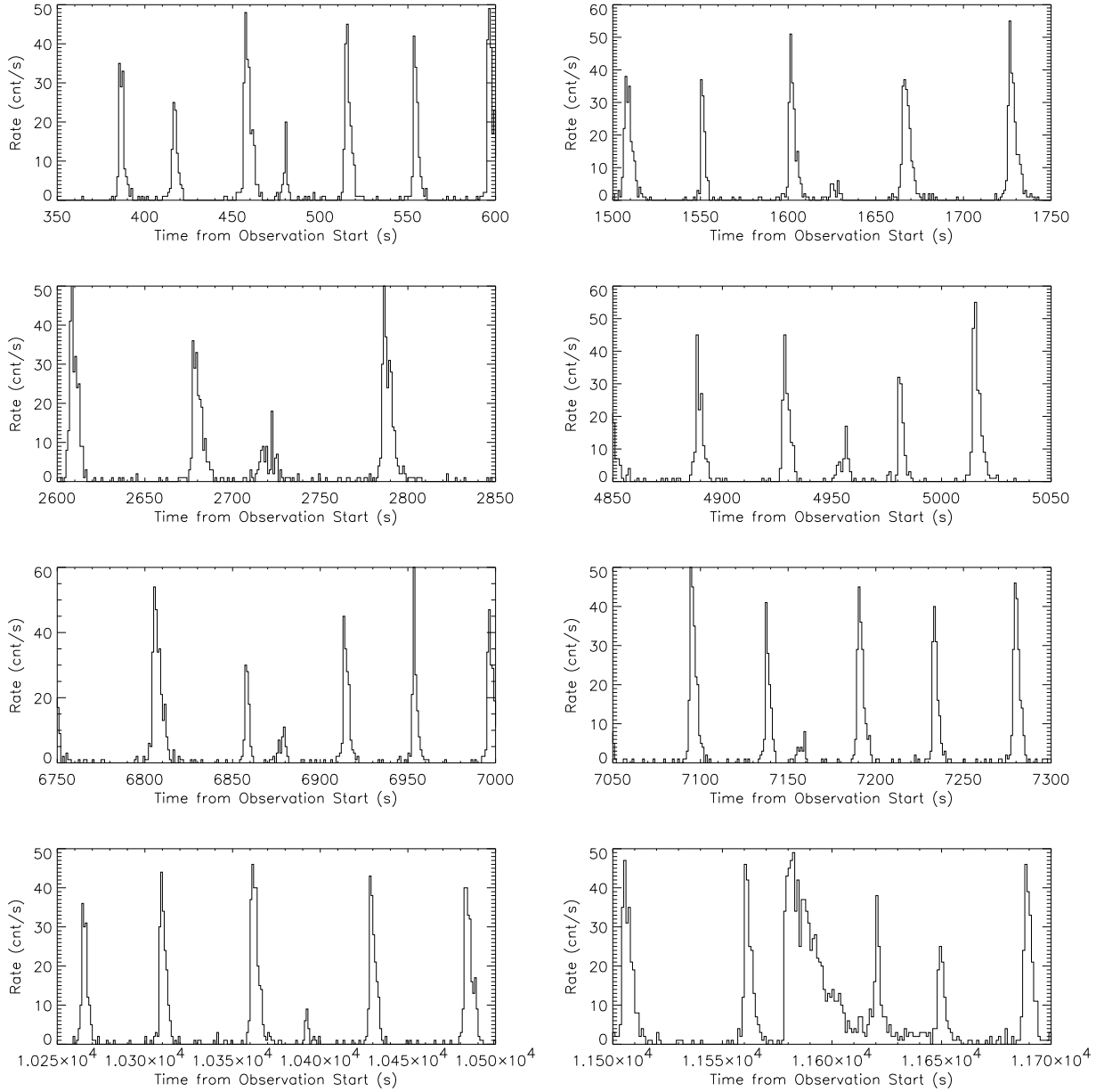


Fig. 1.— Segments of the light curve from zeroth order. The times are offset to the beginning of the observation. Most of the bursts are the normal type II bursts from the Rapid Burster. Near the midpoint of the time interval shown in the first seven panels there is a “mini-burst” where the peak count rate is 5-40% of the average of the normal type II bursts. The bottom right panel shows the type I burst; the tail is so long that two type II bursts are observed during the decay of the type I burst.

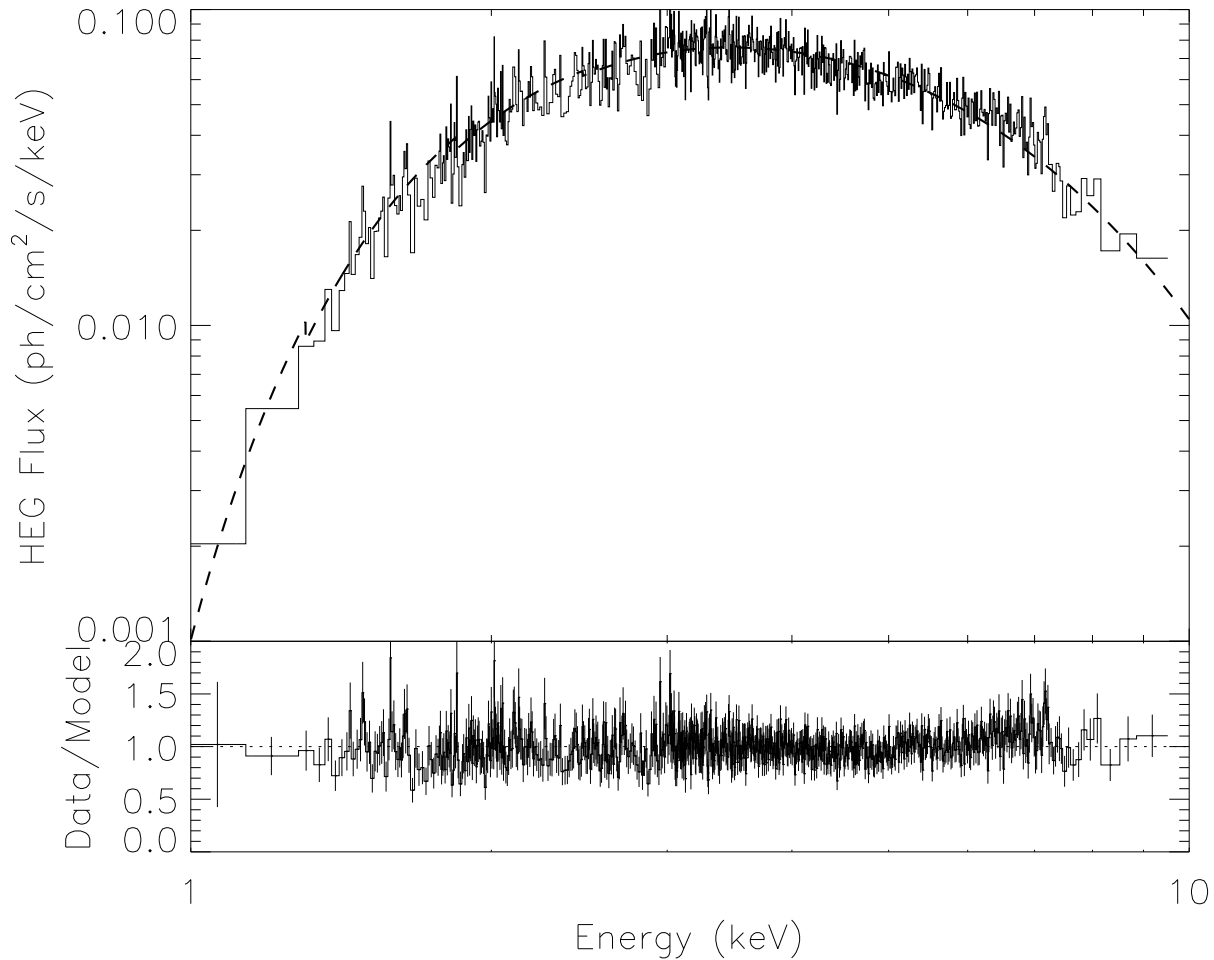


Fig. 2.— Average burst spectrum from the high energy gratings (HEG)s on the *Chandra* HETGS. The data have been adaptively smoothed to give a nearly constant signal/noise ratio. A blackbody model has been fit to the data and overplotted in the upper panel. The data/model ratio is shown in the lower panel, along with the 1σ uncertainties. There are no clear examples of narrow emission or absorption features.

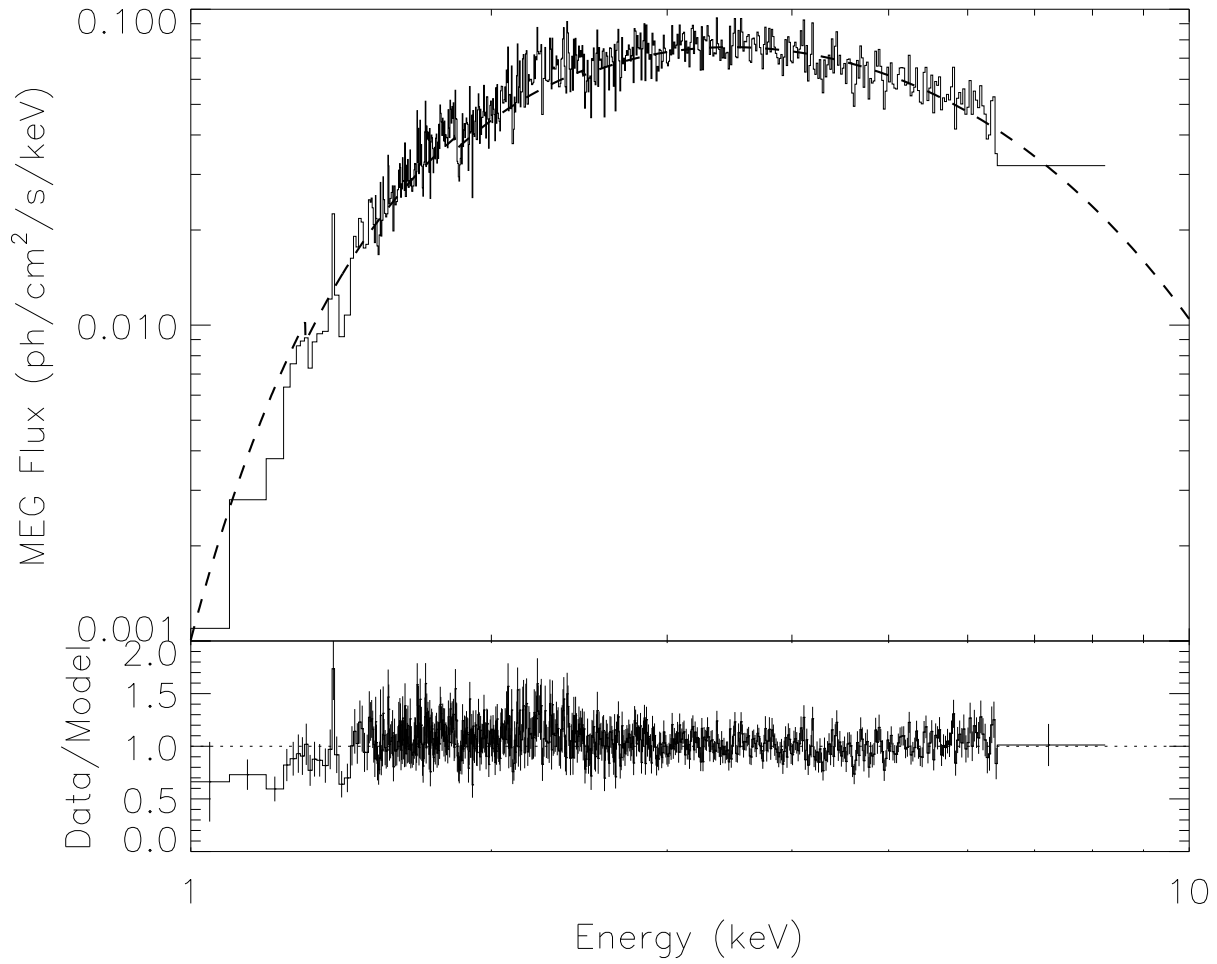


Fig. 3.— Same as Fig.2 except for the medium energy gratings (MEGs) on the *Chandra* HETGS. Again, there are no clear examples of narrow emission or absorption features.

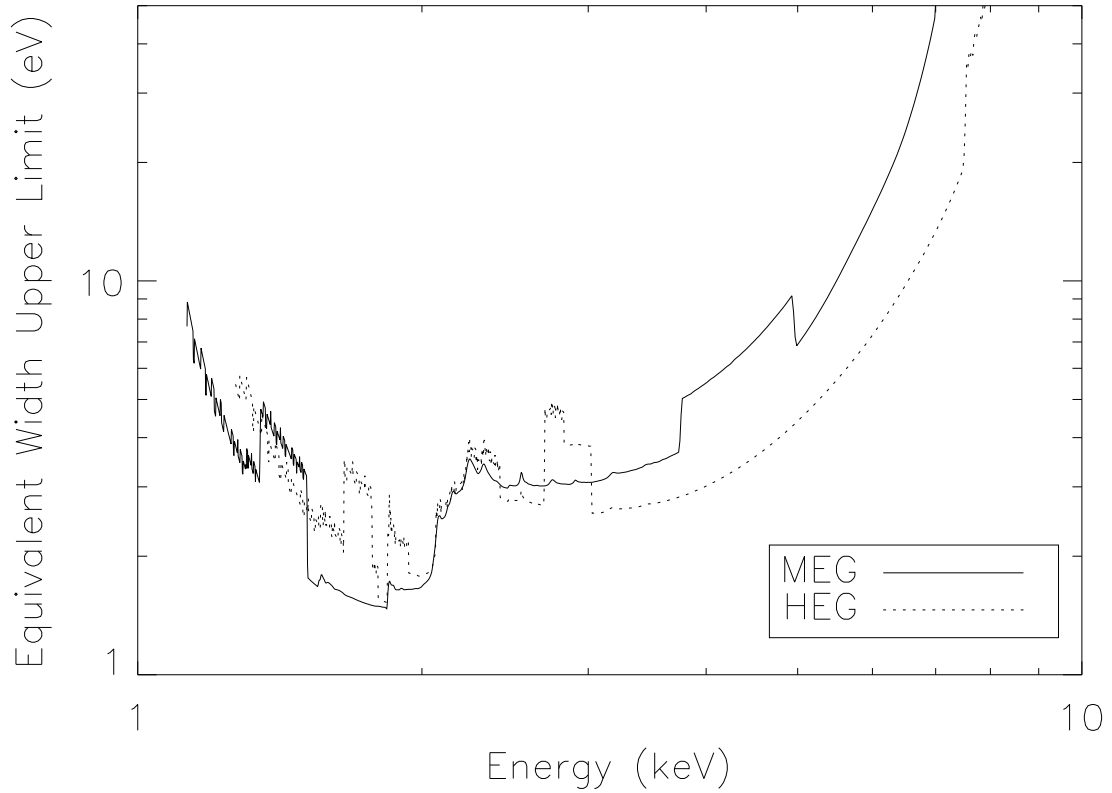


Fig. 4.— Estimates of the 3σ limits that can be placed on any emission lines whose FWHMs are comparable to the instrument resolution. The computation uses the model fitted to the time-averaged HEG and MEG data and the effective areas. We assume that candidate features are only 2 bins wide. The curves are rather smooth, except for locations of chip gaps, so one may derive limits on broad features using these curves until the scale of the feature becomes comparable to that of the instrument calibration uncertainties. Limits on absorption features are identical when there are many counts but are systematically larger at the high and low ends of the spectrum where there are less than 25 counts per bin.